

# Catalytic decomposition of alcohols over size-selected Pt nanoparticles supported on ZrO<sub>2</sub>: A study of activity, selectivity, and stability

S. Mostafa<sup>a,b</sup>, Jason R. Croy<sup>a</sup>, H. Heinrich<sup>a,c</sup>, B. Roldan Cuenya<sup>a,b,d,\*</sup>

<sup>a</sup> Department of Physics, University of Central Florida, Orlando, FL 32816, United States

<sup>b</sup> Department of Civil, Environmental, and Construction Engineering, University of Central Florida, Orlando, FL 32816, United States

<sup>c</sup> Advanced Materials Processing and Analysis Center, University of Central Florida, Orlando, FL 32816, United States

<sup>d</sup> Nanoscience and Technology Center, University of Central Florida, Orlando, FL 32816, United States

## ARTICLE INFO

### Article history:

Received 24 April 2009

Accepted 18 July 2009

Available online 25 July 2009

### Keywords:

Pt  
Nanoparticles  
ZrO<sub>2</sub>  
Catalyst  
Methanol  
Ethanol  
Propanol  
Butanol  
Mass flow reactor  
Mass spectrometry

## ABSTRACT

This article discusses the performance of ZrO<sub>2</sub>-supported size-selected Pt nanoparticles for the decomposition of methanol, ethanol, 2-propanol, and 2-butanol. The potential of each alcohol for the production of H<sub>2</sub> and other relevant products in the presence of a catalyst is studied in a packed-bed mass flow reactor operating at atmospheric pressure. All the alcohols studied show some decomposition activity below 200 °C which increased with increasing temperature. In all cases, high selectivity towards H<sub>2</sub> formation is observed. With the exception of methanol, all alcohol conversion reactions lead to catalyst deactivation at high temperatures ( $T > 250$  °C for 2-propanol and 2-butanol,  $T > 325$  °C for ethanol) due to carbon poisoning. However, long-term catalyst deactivation can be avoided by optimizing reaction conditions such as operating temperature.

© 2009 Elsevier B.V. All rights reserved.

## 1. Introduction

The decomposition of alcohols over metal and metal oxide catalysts has been the subject of numerous studies due to its applicability to a variety of chemical synthesis processes [1–5]. In recent years, this subject has gained particular interest due to growing environmental, economic, and political concerns regarding energy production [2]. Safe and efficient *in situ* hydrogen generation from alcohols (i.e. methanol, ethanol, propanol, butanol) can promote the use of fuel cells and other clean technologies as a source of energy for mobile applications. Alcohols can serve as H<sub>2</sub> carriers that are compatible with current infrastructures for liquid fuels and can be catalytically decomposed on-site in order to minimize energy input requirements and operating temperatures [6].

Catalysts that promote methanol (MeOH) and ethanol oxidation processes are key in the improvement and optimization of

direct MeOH and ethanol fuel cells [6–13] as well as direct H<sub>2</sub> fuel cells, for which decomposition catalysts are also of great importance. Since ethanol can be produced from the fermentation of biomass [7], it is a potentially renewable fuel that can be reformed on-site to generate H<sub>2</sub>. The decomposition of higher order alcohols such as 2-propanol and 2-butanol can also be of interest for a variety of hydrogen-based energy applications while generating other products, i.e. acetone and butanone, which are of great importance in the chemical synthesis industry [14,15]. By increasing activity and selectivity, industrial catalysts can decrease the energy input required as well as the output of potentially harmful by-products associated with numerous chemical processes. Furthermore, it has been shown that the addition of H<sub>2</sub> to fuel mixtures enhances the efficiency and lowers harmful emissions of internal combustion engines [16,17]. Catalytic reforming of gasoline additives, e.g. methanol, ethanol, and potentially butanol, may serve as an on-board source of hydrogen [18]. Waste streams from industries that make use of solvents may contain significant amounts of alcohols and other organics used for this purpose and may require special treatment. Recent studies have focused on the feasibility of obtaining hydrogen (via steam reforming) from 2-propanol, 2-butanol, and other widely used solvents to be used in stationary fuel cell applications [19,20].

\* Corresponding author at: Department of Physics, University of Central Florida, 4000 Central Florida Blvd, MAP 310, Orlando, FL 32816, United States  
Tel.: +1 4078231883.

E-mail address: [roldan@physics.ucf.edu](mailto:roldan@physics.ucf.edu) (B. Roldan Cuenya).

Dehydrogenation of these higher order alcohols may bring the same benefits (i.e. reduction of waste and H<sub>2</sub> production) while generating other valuable products for industrial applications. Efficient catalysts for the dehydrogenation of higher order alcohols may also contribute to improvements in chemical heat pumps, such as those based on the 2-propanol/acetone/hydrogen cycle [21,22].

Methanol decomposition has been shown to take place over a variety of metal surfaces and nanocatalysts including Pt, Pd, Au, Rh, Ni, Co, and Cu supported on metal oxides such as Al<sub>2</sub>O<sub>3</sub>, CeO<sub>2</sub>, ZrO<sub>2</sub>, ZnO, TiO<sub>2</sub>, and SiO<sub>2</sub> [9,12,23–43]. In the absence of O<sub>2</sub> and water, MeOH decomposition favors the formation of H<sub>2</sub> and CO, which can be further reacted in the presence of water to form additional H<sub>2</sub> and CO<sub>2</sub> through the water-gas shift reaction. Platinum has been shown to have good activity and selectivity towards H<sub>2</sub> formation. Previous studies from our group on the decomposition of MeOH over similarly sized Pt nanoparticles (NPs) deposited on SiO<sub>2</sub>, Al<sub>2</sub>O<sub>3</sub>, CeO<sub>2</sub>, TiO<sub>2</sub>, and ZrO<sub>2</sub> [29] revealed an enhanced activity for the Pt/ZrO<sub>2</sub> system.

Ethanol decomposition and the associated reactions including ethanol oxidation and steam reforming have also been thoroughly studied over Pt, Pd, Rh, Cu, Co, Ir, Ni, Fe, and other catalysts supported on CeO<sub>2</sub>, Al<sub>2</sub>O<sub>3</sub>, ZrO<sub>2</sub>, ZnO, and CuO [7,13,18,44–63], and good selectivity towards hydrogen has been observed in several of these systems. The choice of support and the presence or absence of reactants such as O<sub>2</sub> and water, will determine the reaction's selectivity. Pt/CeO<sub>2</sub> and Pt/ZrCeO<sub>2</sub> catalysts tend to promote the formation of H<sub>2</sub> and acetaldehyde [64] and it has been found that these reducible supports enhance catalyst stability [54].

The decomposition of propanol and butanol is carried out in the chemical synthesis industry over Cu-, Zn-, and Ni-based catalysts as well as Pt/Al<sub>2</sub>O<sub>3</sub>. However, concerns for the fate of some of the most commonly used catalysts for this purpose, such as copper chromite, and their environmental impact have provided a motivation to further study and optimize alternative catalysts that may serve this purpose efficiently. In addition, the opportunity of using these alcohols for hydrogen generation to serve as an energy source has placed particular emphasis on finding catalysts that display high conversion and selectivity towards H<sub>2</sub> formation as well as long-term stability. Some studies describing the decomposition of higher order alcohols, i.e. 2-propanol and 2-butanol, over metallic films (Pd–Ag) [65], micrometer-sized powders (Co, Cu, Mg<sub>2</sub>Cu, Ni, metal oxides) [66–72], and supported NPs (Pt, Cu, Pt–Cu, copper chromite, W) [73–80] can be found in the literature.

In order to assess the potential of catalyzed alcohol decomposition we have conducted a systematic study of these reactions over size-selected Pt NPs supported on ZrO<sub>2</sub>. The objective of this study is to assess the catalytic performance (activity, selectivity, and lifetime) of novel, micelle-synthesized, Pt catalysts. The conversion and selectivity of each C1–C4 alcohol was evaluated over a range of temperatures (100–300 °C) under atmospheric pressure in a packed-bed mass flow reactor interfaced to a mass spectrometer. Catalyst stability was monitored through a prolonged exposure to the reactants and insight into the origin of their deactivation at high temperature due to carbonaceous species poisoning was evaluated by X-ray photoelectron spectroscopy (XPS). The by-products of the decomposition reactions are also investigated in order to assess the potential emissions associated with these processes as well as opportunities for material recovery in industrial applications.

## 2. Experimental

Size-selected platinum nanoparticles were synthesized using inverse-micelle encapsulation [27,28,81]. A SiO<sub>2</sub> substrate was dip-coated in the metal-loaded polymeric solution and treated

with an O<sub>2</sub> plasma (for polymer removal) to allow morphological sample characterization using atomic force microscopy (AFM). Pt particles were deposited via impregnation on our nanocrystalline ZrO<sub>2</sub> support with a nominal Pt loading of 2 wt% Pt. The Pt/ZrO<sub>2</sub> catalyst powder was then annealed in an oxygen environment (50% O<sub>2</sub>, 50% He) in a packed-bed reactor at 500 °C. This treatment results in the removal of the polymeric particle shell.

Transmission electron microscopy (TEM, FEI Tecnai F30) of our powder samples was done after annealing in O<sub>2</sub> as well as after exposure to reactants under the experimental conditions described below. Additionally, chemical characterization of our Pt NP catalysts, including their oxidation state, was conducted by XPS (SPECS GmbH) before and after the exposure to different alcohols using a monochromatic X-ray source (Al K $\alpha$ , 1486.6 eV) operating at energy of 350 W. A flood gun was used to compensate for sample charging and the Zr-3d<sub>5/2</sub> core level of ZrO<sub>2</sub> (182.6 eV) [82] was used as the binding energy reference. The XPS spectra were fitted using the CASA XPS software. The Pt-4f core level region of our NPs was fitted with three different doublets corresponding to metallic Pt (Pt-4f<sub>7/2</sub> at ~71.7 eV), PtO (~73.0 eV), and PtO<sub>2</sub> (~75.3 eV). A Shirley background was subtracted from the raw data and slightly asymmetrical line shapes (asymmetry factor = 0.2) were used. Estimated errors of peak positions and spectral area are  $\pm 0.2$  eV and  $\pm 3\%$ .

The catalytic performance of our zirconia-supported Pt NPs in the decomposition of C1–C4 alcohols was evaluated in a packed-bed mass flow reactor. The reactor consists of a 7.4 mm (inner diameter) stainless steel (SS) tube where 100 mg of the catalyst sample is placed and supported by quartz wool. The temperature of the reactor tube is monitored by a K-type thermocouple placed in contact with the reactor wall. Mass flow controllers (MKS) were used to flow He through a stainless steel bubbler, containing the desired alcohol, as well as through a bubbler-bypass line which was used to control the concentration of the alcohols in the feed. The total flow in each experiment was 50 ml/min (at standard conditions) resulting in an alcohol flow of 38  $\mu$ mol/min. The composition of the gas exiting the reactor is monitored using a quadrupole mass spectrometer (QMS, HIDEN, HPR-20) which is connected to the reactor outlet via a heated capillary tube. Changes in the partial pressures of the alcohols and their associated products were used to determine activity (alcohol conversion) and selectivity over temperatures ranging between 100 °C and 300 °C. Each reactant and product was monitored via mass spectrometry based on the mass-to-charge ratios ( $m/z$ ) of their ionized fragments. Mass overlap of reactants and product fragments can make mass spectral analysis difficult. However, each gas has a unique fragmentation pattern within the ionization chamber of the mass spectrometer, and although some of the species studied here have common ion fragments, they also have unique fragments that make their distinction unequivocal. To address this point, a total of 16–22 different masses were monitored simultaneously during each experiment. The main fragments used to identify the reactants include  $m/z$  31 for the methanol and ethanol experiments, and  $m/z$  45 for 2-propanol and 2-butanol. A partial list of the products being monitored to establish selectivity (and the  $m/z$  values of some of their main fragments) includes H<sub>2</sub> (2), CO (28), CO<sub>2</sub> (44), H<sub>2</sub>O (18), CH<sub>4</sub> (15, 16), acetaldehyde (29, 43), acetone (43, 58), propene (39, 41), butanone (43, 72), and butene (41, 56). In addition, the mass spectrometer offers greater sensitivity to oxygenated compounds, as opposed to traditional flame ionization detectors (FID), making it especially suited for the study of higher order alcohols.

Instrumental (QMS) sensitivity factors for reactants and products must be carefully selected for any system. The values used in our work were either taken from a standard library

(MASSoft, Hidden Analytical Inc.) or specifically determined in separate experiments under our experimental conditions. With these factors determined, and the flow of the carrier gas (He) known, partial pressures obtained by the QMS are a direct measure of the flow of each gas in the system (i.e. mol/min). Any conversion of the different alcohols should be accompanied by a corresponding increase in the combined masses of the respective products. After calibration of our instrument we see that this is the case within an error of  $\pm 10\%$ . Thus, selectivity for each product gas detected is given in  $\mu\text{mol/s/g}$  Pt catalyst.

Measurements taken at a catalyst temperature of  $100\text{ }^\circ\text{C}$  were used as reference to ensure that vapors were not condensing within the reactor. In addition, reactivity experiments were also conducted on the Pt-free  $\text{ZrO}_2$  support and on the blank SS reactor (containing only quartz wool) for each alcohol. The blank SS reactor tube was found to display low reactivity below  $300\text{ }^\circ\text{C}$  ( $<7\text{--}17\%$  for all alcohols), and such data have been subtracted from the reactivity of the Pt/ $\text{ZrO}_2$  and  $\text{ZrO}_2$  samples in Figs. 6 and 7. Each experiment was carried out two times in order to test the reproducibility of the reactivity results obtained, and the average values, along with error bars, are shown in the figures. The error was calculated as the difference between the minimum and maximum values obtained from the repeated experiments. The error margins shown in Fig. 6(a) and (b) represent the error in the blank experiments plus the error in the Pt/ $\text{ZrO}_2$  data and the  $\text{ZrO}_2$  data, respectively. In order to study the potential deactivation of our catalysts under reaction conditions, the reactor temperature was elevated up to  $400\text{ }^\circ\text{C}$  and indications of deactivation (i.e. decreased activity) were monitored. Above  $300\text{ }^\circ\text{C}$ , accurate quantitative estimations of catalyst performance become difficult due to the convolution of the catalytic activity of our samples with that associated with the SS reactor walls as well as gas-phase reactions. Therefore, our discussion related to the activity in the  $300\text{--}400\text{ }^\circ\text{C}$  temperature range is limited to a qualitative description of clearly discernable trends in catalytic activity. Long-term stability was determined by exposure to the alcohols under reaction conditions for a period of 17 h as described in the stability section.

### 3. Results

#### 3.1. Catalyst characterization

##### 3.1.1. Morphology (AFM, TEM)

The AFM image in Fig. 1 reveals the narrow size distribution of our as prepared Pt nanoparticles when dip-coated on  $\text{SiO}_2/\text{Si}(0\ 0\ 1)$ . This micrograph was acquired after polymer removal in UHV by  $\text{O}_2$  plasma. The average NP height was found to be  $2.1 \pm 0.4\text{ nm}$ .

The TEM images shown in Fig. 2 (overview) and Fig. 3 (high resolution) show the as prepared Pt NPs deposited on the  $\text{ZrO}_2$  support after annealing in  $\text{O}_2$  and before reaction with the different alcohols [Figs. 2(a) and 3(a)], and after reaction with methanol [Figs. 2(c) and (d) and 3(b)], ethanol [Figs. 2(e) and 3(c)], 2-propanol [Figs. 2(b) and 3(d)], and 2-butanol [Figs. 2(f) and 3(e)]. Our TEM images demonstrate a narrow particle size distribution over the zirconia surface before and after the different reactions. Based on the high resolution TEM images (Fig. 3), the average particle diameter in these samples is  $4.8 \pm 1.0\text{ nm}$ . The difference between the NP height obtained from AFM images and the diameter observed in the TEM images may result partly from morphological changes occurring upon annealing, due to strong nanoparticle-support interactions, causing the particles to take a hemispherical shape. No significant change in the average size is observed when comparing samples before and after exposure to reactants at temperatures up to  $400\text{ }^\circ\text{C}$  (Fig. 3), indicating that coarsening is

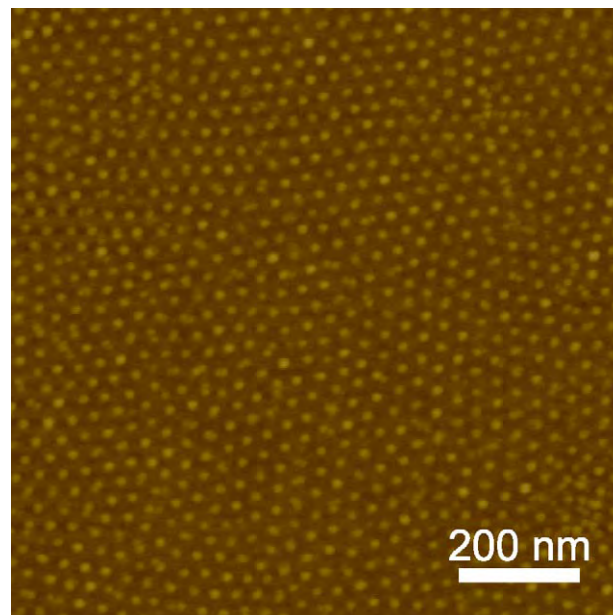


**Fig. 1.** *Ex situ* AFM image of Pt nanoparticles synthesized by encapsulation in PS(27700)-PV2P(4300) and dip-coated on  $\text{SiO}_2/\text{Si}(0\ 0\ 1)$ . The polymer shell was removed by an  $\text{O}_2$  plasma treatment for 2 h at  $4.5 \times 10^{-5}$  mbar  $\text{O}_2$ .

not taking place during the different reactions. However, an amorphous layer not present in the fresh sample [after  $\text{O}_2$  annealing, Fig. 3(a)], is observed by TEM in the catalyst sample exposed to ethanol, Fig. 3(c), and to a certain extent also in those exposed to 2-propanol and 2-butanol [Fig. 3(d) and (e), respectively]. This layer indicates the deposition of carbonaceous species during C2–C4 decomposition, as will be shown in connection with XPS data.

##### 3.1.2. Chemical composition (XPS)

XPS measurements were used to determine the oxidation state of the as-prepared Pt nanocatalysts and to monitor possible changes in this state after reactions. Fig. 4 displays fitted XPS spectra of the Pt-4f core level region of the Pt/ $\text{ZrO}_2$  catalyst before and after reactions with alcohols (at temperatures up to  $400\text{ }^\circ\text{C}$ ) as given by the right-hand side labels. Vertical lines in Fig. 4 denote the approximate position of the Pt-4f<sub>7/2</sub> components of Pt<sup>0</sup> in metallic Pt at 71.7 eV (solid line) [28], Pt<sup>2+</sup> in PtO at 73.0 eV (dashed line) [83], and Pt<sup>4+</sup> in PtO<sub>2</sub> at 75.3 eV (dashed line) [83]. A shift with respect to the position of bulk metallic platinum from 71.1 eV to  $\sim 71.7\text{ eV}$  is observed for the metallic Pt component, which is consistent with previous observations by our group [28] and is attributed to particle size effects [81,84–86] and/or the formation of Pt–Zr, Pt–Zr–O alloys [87]. Catalyst exposure to all alcohols, and the associated sample heating up to  $400\text{ }^\circ\text{C}$ , resulted in a strong reduction of Pt oxide species, although complete reduction was never observed. Table 1 shows the relative content of the different Pt species before and after alcohol exposure as determined by the area under the corresponding fitted doublets (Pt 4f<sub>7/2</sub> and 4f<sub>5/2</sub> core levels). It can be observed that Pt oxides make up over 50% of the total platinum species in the as-prepared sample (after annealing in  $\text{O}_2$ ) and at least 10% of those present after exposure to reactants.

XPS measurements from the C-1s region conducted on the Pt/ $\text{ZrO}_2$  catalyst and the Pt-free  $\text{ZrO}_2$  support are displayed in Fig. 5(a) and (b), respectively. The bottom spectra in these figures represent the fresh Pt/ $\text{ZrO}_2$  and  $\text{ZrO}_2$  samples and the remaining spectra correspond to measurements conducted after exposure to the different alcohols as indicated by the left-hand side labels. All spectra are plotted using the same scale but are displaced vertically for clarity. Only a very small C signal, associated with adventitious

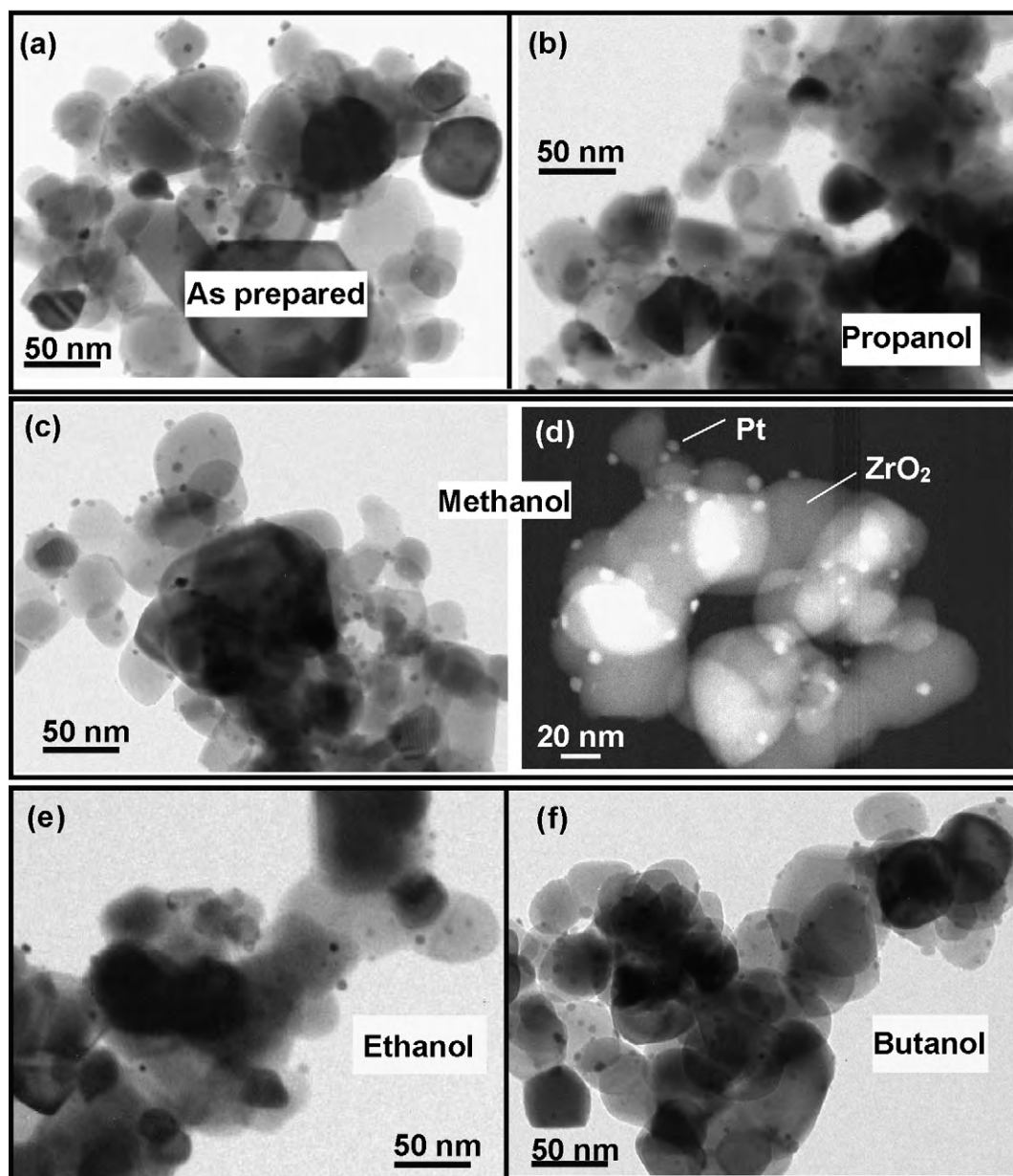


**Fig. 2.** Low magnification TEM images of the Pt/ZrO<sub>2</sub> catalysts: (a) as prepared (only exposed to a pre-treatment in O<sub>2</sub> at 500 °C for 4 h) and after exposure to 2-propanol (b), methanol (c and d), ethanol (e), and butanol (f), each of them at 400 °C for up to 10 h. The image shown in (d) displays atomic number contrast, with lighter areas (excluding the regions of oversaturation due to the presence of multiple layers of the ZrO<sub>2</sub> powder) corresponding to the element with higher atomic number (Pt).

carbon, is observed in the fresh samples (labeled “as prepared”), indicating the removal of the encapsulating polymer from the Pt/ZrO<sub>2</sub> sample by the O<sub>2</sub> annealing pre-treatment [88]. Interestingly, after exposure to MeOH the ZrO<sub>2</sub> and Pt/ZrO<sub>2</sub> samples remain carbon-free, while a large increase in the C-1s intensity is observed after ethanol, 2-propanol, and 2-butanol exposure. The C-1s spectra of all the samples were fitted using three different photoelectron peaks, Fig. 5. The first peak at ~285 eV corresponds to the presence of carbon species predominantly containing bonds of the type C–C and C–H (e.g. hydrocarbons, C<sub>x</sub>H<sub>y</sub>) [82,89]. The second peak at ~286 eV is assigned to the presence of oxygenated carbonaceous species (C–OH/C–OR) [82], and the third peak at ~289.8 eV is assigned to carboxyl and/or carbonate species over the catalyst surface [82,89–91]. The C signals detected in the Pt/ZrO<sub>2</sub> samples exposed to C2–C4 alcohols are in agreement with the amorphous thin layers observed in the TEM images of some of these samples, Fig. 3, and they also correlate to the trends in activity and selectivity that will be

discussed in the next sections. Based on a literature comparison, possible origins for the carbonaceous species detected by XPS are included in the discussion section.

### 3.2. Catalyst performance

#### 3.2.1. Activity

In order to evaluate the activity of our catalyst for alcohol decomposition, the conversion taking place over a range of temperatures between 100 °C and 300 °C was calculated. The conversion of each alcohol over the catalyst was calculated according to the formula:

$$\frac{P_i - P_T}{P_i} \times 100, \quad (1)$$

where  $P_i$  represents the partial pressure of each alcohol in the reactor (measured by a mass spectrometer) at a reference

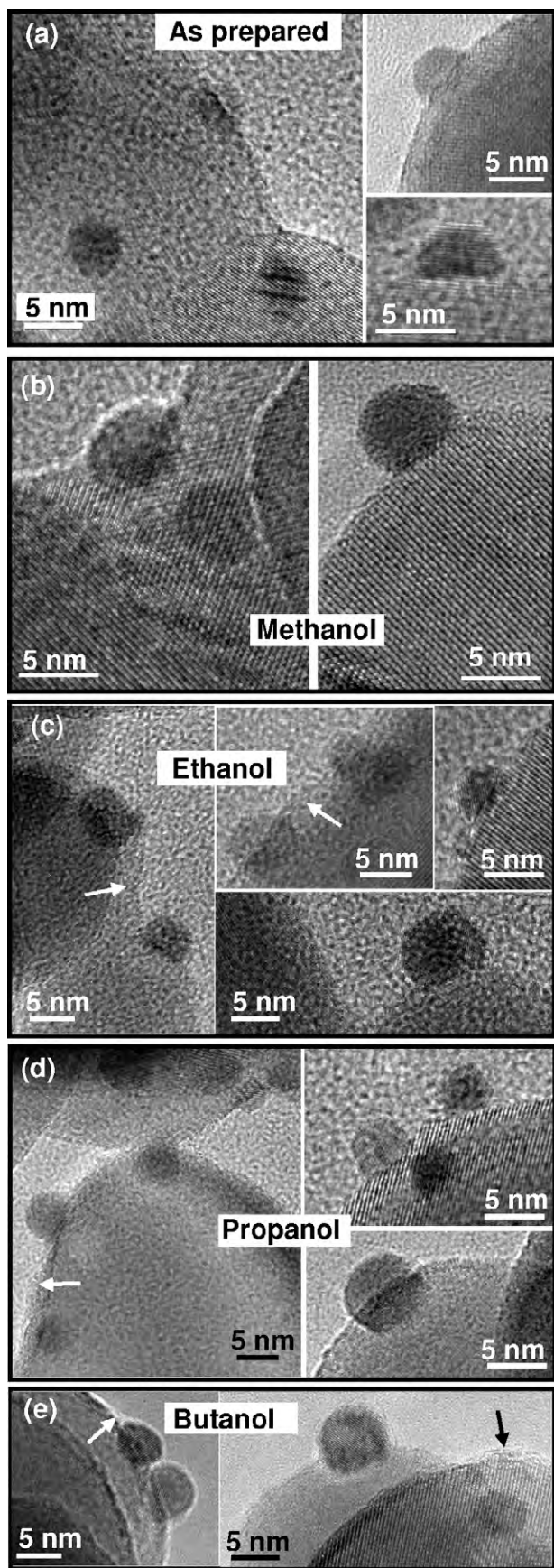


**Fig. 3.** High resolution TEM images of the Pt/ZrO<sub>2</sub> catalysts as prepared (only exposed to a pre-treatment in O<sub>2</sub> at 500 °C for 4 h) (a) and after exposure to methanol (b), ethanol (c), 2-propanol (d) and 2-butanol (e), each of them at 400 °C

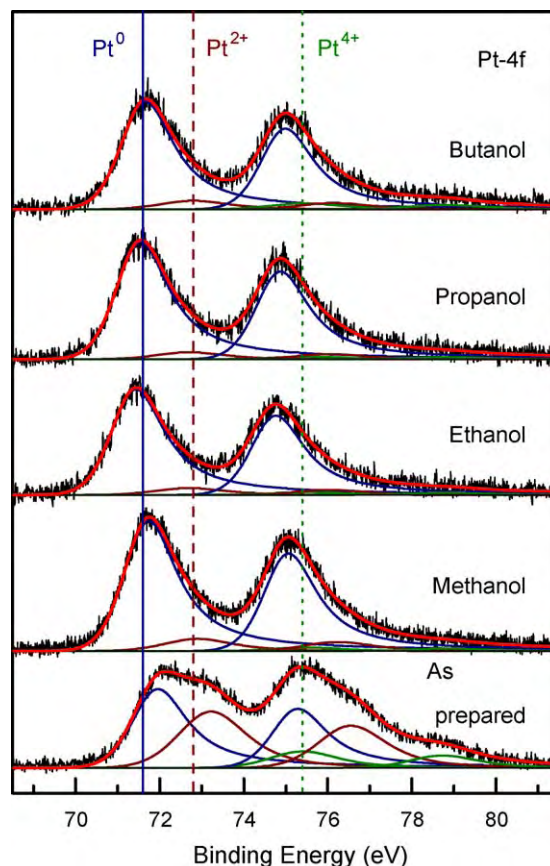


**Fig. 4.** XPS spectra of the Pt-4f core level region of a fresh Pt/ZrO<sub>2</sub> sample after a pre-treatment in oxygen at 500 °C for 4 h (as prepared sample), and analogously synthesized samples after subsequent exposure to methanol, ethanol, 2-propanol and 2-butanol at a maximum temperature of 400 °C for up to 10 h. The reference lines indicate the binding energy of the 4f<sub>7/2</sub> core level of metallic Pt (solid line), PtO (dashed line), and PtO<sub>2</sub> (dotted line).

temperature of 100 °C, and  $P_T$  represents the partial pressure at a given temperature,  $T$ . The conversion for each of the alcohols as a function of temperature is shown in Fig. 6(a) for the Pt NPs supported on ZrO<sub>2</sub>, and in Fig. 6(b) for the Pt-free nanocrystalline ZrO<sub>2</sub> support, both after exposure to an identical thermal pre-treatment in oxygen.

As expected, based on previous studies by our group on similarly prepared catalysts [27,29], methanol was efficiently decomposed over the Pt/ZrO<sub>2</sub> catalyst, Fig. 6(a). The onset of methanol conversion occurs at a temperature of about 175 °C, and the activity was found to increase with temperature, reaching over 90% conversion at 300 °C. Beyond that temperature, complete conversion and no deactivation for at least 10 h (time frame of our reactivity experiment) were observed. Ethanol conversion over Pt/ZrO<sub>2</sub> was found to start at ~150 °C, increasing with increasing temperature up to about 47% conversion at 300 °C, Fig. 6(a). Catalytic activity decreases sharply above 325 °C (not shown). 2-Propanol and 2-butanol displayed the lowest onset temperature of ~125 °C and were effectively decomposed throughout the entire temperature range showing similar trends in terms of conversion, Fig. 6(a). After reaching maxima in activity at ~250 °C, some catalyst deactivation takes place as demonstrated by a decrease in the conversion activity of both alcohols with increasing tempera-

ture for up to 10 h. The presence of an amorphous layer over the catalyst surface (not present over the fresh and methanol-exposed samples) is indicated in figures (c–e) by arrows. Such layer is assigned to the depositions of carbonaceous species during exposure to reactants.

**Table 1**

Pt, PtO and PtO<sub>2</sub> content (%) of our as prepared Pt/ZrO<sub>2</sub> catalysts after annealing at 500 °C in oxygen for 4 h and subsequent exposure to methanol, ethanol, propanol and butanol obtained from the analysis of XPS data.

Exposure	Pt <sup>0</sup> B.E. (eV)	Pt <sup>0</sup> (%)	PtO (%)	PtO <sub>2</sub> (%)
4 h O <sub>2</sub>	72.0	46	42	12
Methanol	71.7	86	11	3
Ethanol	71.4	89	8	3
2-Propanol	71.5	90	3	
2-Butanol	71.7	85	9	6

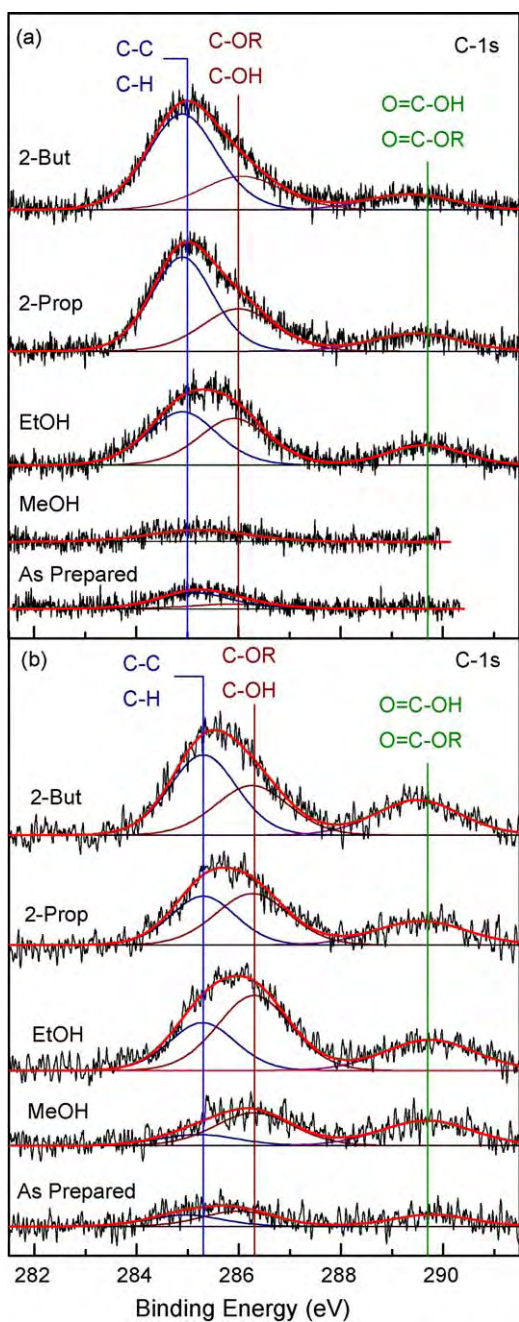


**Fig. 5.** XPS spectra of the C-1s core level region of (a) our nanoscale Pt/ZrO<sub>2</sub> catalysts and (b) the Pt-free ZrO<sub>2</sub> support, as prepared (only exposed to a pre-treatment in O<sub>2</sub> at 500 °C for 4 h) and after exposure to methanol, ethanol, 2-propanol and 2-butanol at 400 °C for up to 10 h. The reference lines indicate the binding energies of different carbonaceous species: C-C/C-H (~285 eV), C-OR/C-OH (~286 eV), and O=C-OH/O=C-OR (~289.8 eV). The spectra are presented vertically displaced for clarity.

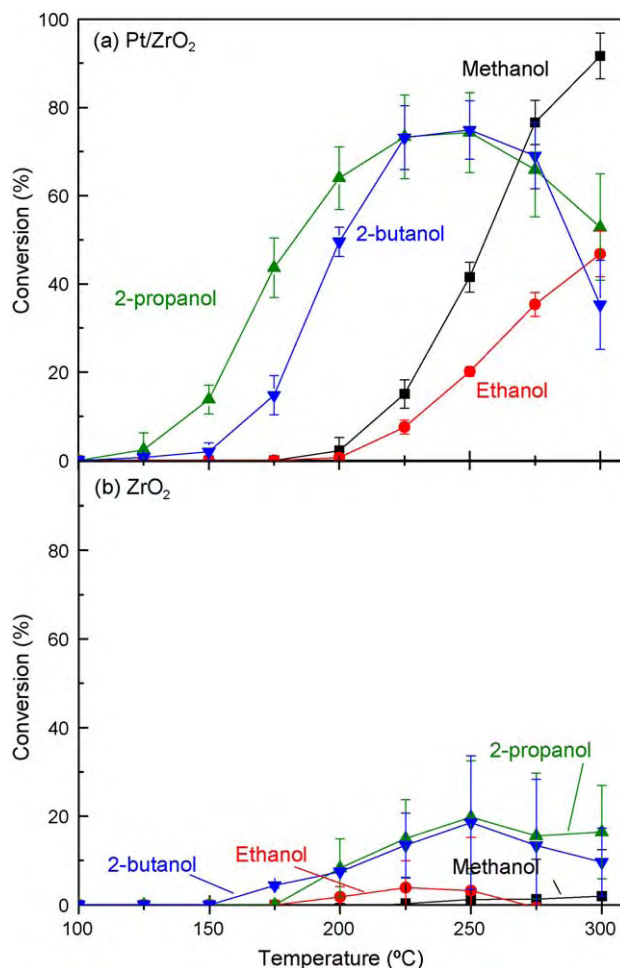


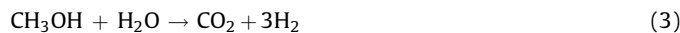
**Fig. 6.** Temperature-dependent alcohol decomposition data obtained in a packed-bed mass flow reactor interfaced to a mass spectrometer. The data in (a) correspond to Pt nanoparticles deposited on nanocrystalline ZrO<sub>2</sub> while (b) displays the reactivity of the Pt-free ZrO<sub>2</sub> support.

ture up to 300 °C. The conversion of the different alcohols over the Pt-free ZrO<sub>2</sub> support was relatively low (2–20%) as compared to the activity observed in the presence of Pt (47–92%).

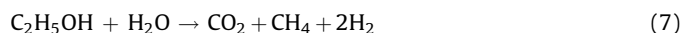
### 3.2.2. Selectivity

Catalyst selectivity was monitored with a particular interest in its ability to generate H<sub>2</sub> from C1–C4 alcohols. The dominant reaction pathways observed in the decomposition of each of the alcohols studied are described below. Eqs. (2)–(5) correspond to methanol decomposition, Eqs. (6)–(10) to ethanol, Eqs. (11) and (12) to 2-propanol, and Eqs. (13) and (14) to 2-butanol decomposition.

Methanol decomposition and related reactions:



Ethanol decomposition and related reactions:

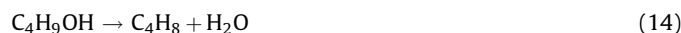




2-propanol dehydrogenation and dehydration:



2-butanol dehydrogenation and dehydration:



Selectivity towards the different products was determined based on our mass spectrometry data. Fig. 7 shows the rate of (a) methanol, (b) ethanol, (c) 2-propanol, and (d) 2-butanol conversion in units of  $\mu\text{mol/s g}$  catalyst (0.1 g Pt/ZrO<sub>2</sub>) (dashed lines) together with the rate of production of H<sub>2</sub> and a variety of reaction by-products (methane, acetone, butanone, etc., solid symbols connected by solid lines).

In the case of methanol, Fig. 7(a), the direct decomposition reaction described by Eq. (2) was greatly favored, with H<sub>2</sub> and CO accounting for nearly 100% of the products generated up to 300 °C.

The conversion data for ethanol and the associated reaction by-products are shown in Fig. 7(b) and may be explained in terms of the pathways suggested above. Ethanol decomposition shows significant H<sub>2</sub> production accompanied by the generation of CO, CH<sub>4</sub>, as well as smaller amounts of CO<sub>2</sub>, water, and acetaldehyde (C<sub>2</sub>H<sub>4</sub>O) for temperatures up to 300 °C. This suggests that reaction (6) is dominant for this temperature range, while pathways (5), (7) and (8) may also occur to a lesser degree.

The selectivity of 2-propanol and 2-butanol decomposition are shown in Fig. 7(c) and (d), respectively. For temperatures below 250 °C high selectivity for H<sub>2</sub> production is observed. The reactions observed in this temperature range result in the generation of acetone (C<sub>3</sub>H<sub>6</sub>O) in the case of 2-propanol [reaction (11)], and butanone (C<sub>4</sub>H<sub>8</sub>O) for the decomposition of 2-butanol [reaction (13)]. However, the formation of water is observed above 250 °C, indicating the onset of the dehydration reactions [reactions (12) and (14)] for both reactants.

### 3.2.3. Catalyst deactivation and stability

The peak in activity in the decomposition of 2-propanol and 2-butanol ( $T \sim 250$  °C) and the drop in activity that follows is an indication of catalyst deactivation. In the case of ethanol, a similar behavior was observed at  $T > 325$  °C (not shown). On the other hand, the catalytic activity for methanol decomposition remained steady after reaching a conversion >95% for the remainder of the temperatures studied (from  $T \sim 300$  °C up to 400 °C). Therefore, the temperature at which our Pt/ZrO<sub>2</sub> catalyst deactivated was found to be a function of the alcohol being decomposed, possibly related to the temperature at which C–C bond scission takes place, as well as the formation of specific reaction intermediates. In order to distinguish between temperature and time-on-stream effects, stability experiments were conducted where the catalysts were exposed to the reactants for  $\sim 17$  h at temperatures below which short-term deactivation was observed for each alcohol. The temperatures selected for these experiments were 225 °C for methanol, 250 °C for ethanol, and 200 °C for both 2-propanol and 2-butanol. The catalyst's activity in the decomposition of all the alcohols remained constant throughout the duration of each experiment. In addition, selectivities were similar to those reported in the low temperature region (<250 °C) of Fig. 7.

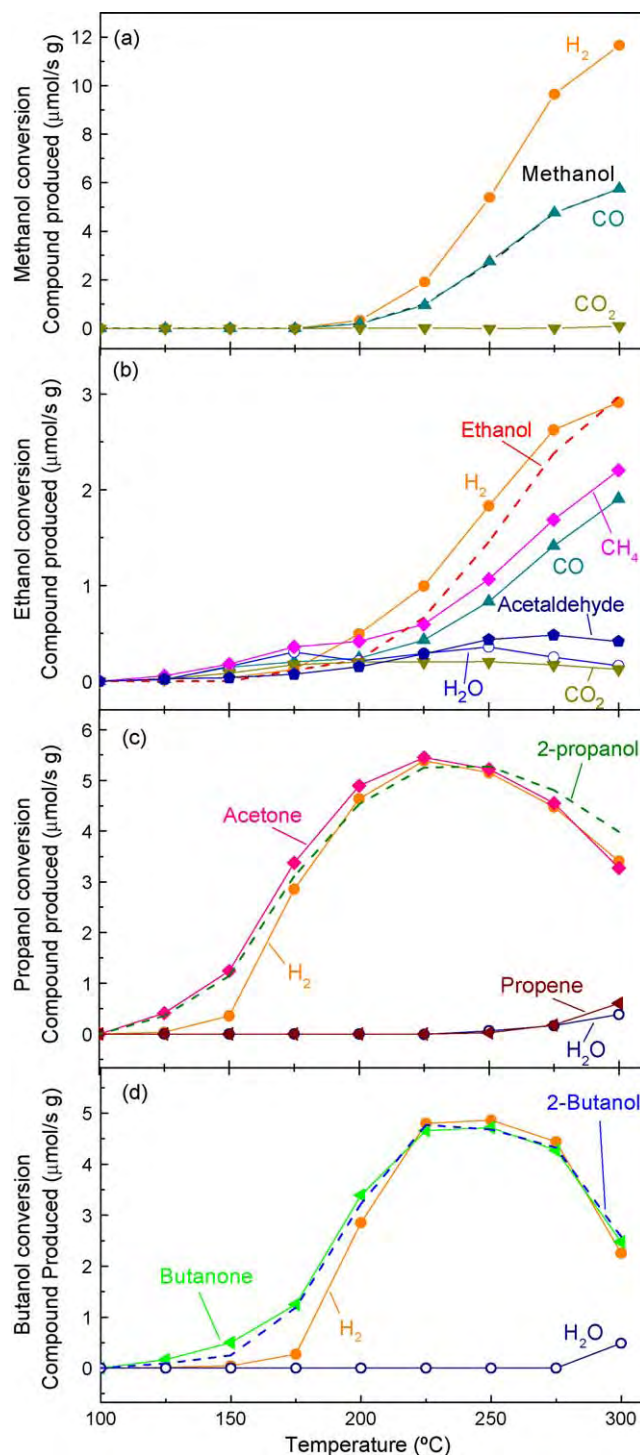


**Fig. 7.** Rate of alcohol decomposition (dashed lines) and production of related by-products over Pt nanoparticles supported on nanocrystalline ZrO<sub>2</sub> (solid lines and closed symbols). The data in (a) correspond to methanol, (b) to ethanol, (c) to 2-propanol, and (d) to 2-butanol decomposition. The rates are normalized by the weight of Pt/ZrO<sub>2</sub> catalyst (in grams) present in each sample ( $\sim 0.1$  g).

## 4. Discussion

As described in Fig. 6(a), all the alcohols studied displayed some conversion over the Pt/ZrO<sub>2</sub> catalyst below 200 °C. Within the 100–200 °C range, 2-propanol followed by 2-butanol display the greatest conversion. At 225 °C, over 70% of the 2-propanol and 2-butanol introduced is being catalytically converted. Over the Pt-free ZrO<sub>2</sub> support [Fig. 6(b)], 2-propanol and 2-butanol display

higher conversion than methanol and ethanol over the entire temperature range, although at lower rates as compared to the activity over the platinum catalyst. This result may seem unexpected if we consider that it requires more energy to break the C–C bonds present in the higher order alcohols. However, when we consider the products of these reactions in Fig. 7(a–d) we observe that the conversion of all the alcohols is dominated by hydrogen production. This means that 2-propanol and 2-butanol may undergo dehydrogenation through reactions that do not require C–C bond scission. This assertion is supported by the predominance in the generation of acetone and butanone derived from the 2-propanol [Eq. (11)] and 2-butanol [Eq. (13)] reactions, respectively.

For methanol and ethanol the addition of Pt to the ZrO<sub>2</sub> support does little to improve the activity below 200 °C. However, above this temperature ethanol shows a steady increase in conversion while methanol displays the greatest overall improvement in the range of 200–300 °C. From this we can see that the Pt NPs play a significant role in the decomposition of these alcohols in this temperature range. Our conversion rates and onset temperatures for methanol decomposition are in agreement with previous literature reports [14,24,32–34,36,40]. Selectivity for H<sub>2</sub> and CO appears to depend on the choice of nanoparticle-support, and other catalyst properties (e.g. composition, particle size) and such high selectivity as observed in our experiments has been shown to occur over Pt- and Pd-based catalysts supported on ZrO<sub>2</sub> and CeO<sub>2</sub> as well as activated carbon [14,32,34,36,40]. Supported Pt and Pd particles have been reported to display greater conversion of ethanol over a similar temperature range [46] or displaying slightly lower (~150 °C) onset temperatures for this reaction [45]. Acetaldehyde has been reported to be the dominant product over Pt/CeZrO<sub>2</sub> [47] while ethene is mostly formed over Pt/Al<sub>2</sub>O<sub>3</sub> [46]. These products can be formed without C–C bond scission, which is not the case for the products observed in our experiments. It must be noted that significantly greater conversion rates have been observed over the catalysts mentioned above in the presence of oxygen or steam [44,45,47,48,50,54,55,64].

After reaching >90% conversion at  $T \sim 300$  °C, the rate of MeOH decomposition remains constant for the entire range of temperatures (up to 400 °C), indicating that significant catalyst deactivation is not taking place. XPS data obtained after exposing the Pt/ZrO<sub>2</sub> catalyst to MeOH under reaction conditions up to 400 °C indicate that no detectable amounts of carbon are present on the catalyst surface in excess of those observed before the reaction, Fig. 5. This is interesting in light of the well-known poisoning effects of CO on Pt and may be related to the nature of the strong particle-support interaction in this system and the possible formation of Pt–Zr and/or Pt–Zr–O alloys.

The conversion of ethanol also shows a steady increase in activity up to 300 °C, Fig. 6(a) over the Pt/ZrO<sub>2</sub> catalyst. The detected products indicate that that C–C bond scission is taking place over the catalyst surface and that reaction (6) may compete with the formation and/or desorption of acetaldehyde (C<sub>2</sub>H<sub>4</sub>O) [Eq. (8)], keeping this latter pathway from becoming more prevalent as demonstrated by the smaller amounts of C<sub>2</sub>H<sub>4</sub>O being formed. CO and H<sub>2</sub> may react to form methane and water, and in turn, promote the water-gas shift (4) and ethanol steam reforming (7) reactions. The catalyst undergoes significant deactivation at temperatures greater than 325 °C and similar behaviors have been reported following the poisoning of Pt/Al<sub>2</sub>O<sub>3</sub> catalysts [46] and at  $T \sim 350$  °C over a CuO/Al<sub>2</sub>O<sub>3</sub> [57].

TEM images taken before and after the reactivity experiments (Figs. 2 and 3) indicate that particle sintering is not taking place over the range of temperatures studied. Therefore, increased particle size is not a viable explanation for catalyst deactivation. However, an amorphous layer on the catalyst surface, visible in

Fig. 3(c), indicates the presence of contaminants that may block active sites. These deposits consist mainly of carbonaceous species generated during the decomposition of ethanol as indicated by our XPS measurements of Fig. 5(a) and (b).

It should be noted that without the use of *in situ* surface analysis techniques (e.g. FTIR or DRIFTS) that allow the determination of adsorbed intermediates, a quantitative mechanistic description of the reaction pathways or detailed deactivation phenomena cannot be established. Therefore, we have used well-established related literature as referent to discuss plausible explanations for our experimental observations. In order to understand the deactivation mechanism, the possible reactions taking place must be considered. Ethanol is believed to adsorb on the ZrO<sub>2</sub> surface either molecularly [46] or through dissociative adsorption forming ethoxy species [47]. Loss of hydrogen can lead to the formation of acetaldehyde or acetate species through interaction with the support's oxygen. Interfacial sites where the Pt comes in contact with the oxide support have been proposed as promoters of acetate demethanation and acetaldehyde decomposition [47], both of which may lead to the products observed by us in the case of ethanol decomposition [Fig. 7(b)], namely methane, CO, and H<sub>2</sub>. The accumulation of by-products and/or intermediate species, such as acetate and other oxygenated species, over the catalyst surface can be seen in Fig. 5(a) and (b) represented by peaks located at ~286 eV and ~289.8 eV. The high energy peak at 289.8 eV has been associated with carboxyl moieties or other carbonaceous deposits on the acid sites known as “acidic coke”, which would likely form over the ZrO<sub>2</sub> surface. It has been previously proposed that these adsorbed species hinder the migration of other intermediates over the metal oxide support and prevent them from reaching the catalytically active Pt–ZrO<sub>2</sub> interface [46,92], resulting in their accumulation over the catalyst surface. This explanation satisfies both the deactivation observed over the Pt/ZrO<sub>2</sub> catalyst and the accumulation of oxygenated carbon species over both the Pt/ZrO<sub>2</sub> and the ZrO<sub>2</sub> support. The rate limiting step in this model (i.e. migration of molecules to interfacial sites) precedes the interaction of intermediate species with the Pt particles. Thus, the origin of C<sub>x</sub>H<sub>y</sub> species formed and stabilized in the presence of platinum [peak observed at ~285 eV, Fig. 5(a)] could be attributed to species formed through the interaction of the ethanol molecules directly on the Pt surface. De Lima et al. [47] have recently proposed that the accumulation of oxygenated species over the support surface is not the cause but rather the result of catalyst deactivation caused by the accumulation of CH<sub>x</sub> species at the Pt-support interface. Contamination of these active sites reduces intermediate turnover and causes the build-up of these species over the catalyst surface. This mechanism explains the presence of oxygenated carbon deposits on both the ZrO<sub>2</sub> and the Pt/ZrO<sub>2</sub> catalysts, while the C<sub>x</sub>H<sub>y</sub> are mainly observed when Pt is present.

The conversion activities of 2-propanol and 2-butanol reach their maxima at  $T \sim 250$  °C. Rioux and Vannice [79,80] studied 2-propanol dehydrogenation over C-supported Cu, Pt, and Cu-Pt nanoparticles with the intent of finding high selectivity and conversion comparable to currently used industrial catalysts, yet at lower metal loadings. Our Pt/ZrO<sub>2</sub> catalyst displays higher conversion than their Pt-based catalysts at similar metal loadings and particle size (~4 nm), possibly due to the synergistic interaction between our particles and oxide support, while maintaining very high H<sub>2</sub> selectivity (>90%). The dehydrogenation of 2-butanol has also been investigated mostly over supported copper catalysts [67,74,76,78], which display high selectivity towards H<sub>2</sub> and butanone but lower conversion rates than those observed over our Pt/ZrO<sub>2</sub> catalyst. The performance of the Cu/SiO<sub>2</sub> catalyst in the decomposition of 2-butanol displays structure dependence, as larger particles (>8 nm) show greater activity than

smaller ones [78]. Such size- and structure-dependence in the performance of our Pt/ZrO<sub>2</sub> catalyst in the decomposition and oxidation of higher order alcohols will be the subject of future studies by our group.

During our 2-propanol and 2-butanol experiments, some catalyst deactivation becomes evident at temperatures greater than 250 °C. The deactivation is a function of increased temperature and not time-on-stream alone as demonstrated by our stability tests. Coke formation due to the deposition of carbonaceous species on the metal surface has been reported at temperatures similar to those where conversion is hindered in our study [67,69], and is a possible source of catalyst deactivation at high temperatures. Furthermore, XPS of the C-1s region indicate that both oxygenated carbon species and hydrocarbon species are present in the Pt/ZrO<sub>2</sub> after exposure to 2-propanol and 2-butanol, Fig. 5(a); however the Pt-free support that has been exposed to the same reactants contains carbon deposits predominantly associated with the oxygenated species, Fig. 5(b). 2-Propanol has been shown to adsorb over the ZrO<sub>2</sub> surface in a similar fashion to that of ethanol (i.e. molecular and dissociative adsorption) and to further decompose over this surface leading to the reactions observed in our studies [93,94], while the decomposition activity is enhanced in the presence of Pt [80,94,95]. A parallel could then be drawn between the deactivation mechanism during the ethanol experiments and those involving higher order alcohols, where Pt–ZrO<sub>2</sub> interfacial sites become blocked by C<sub>x</sub>H<sub>y</sub> species, reducing intermediate turnover and leading to the accumulation of oxygenated carbon species over the catalyst surface. Our TEM images [Fig. 3(d) and (e)] display some evidence of carbonaceous deposits over the catalyst surface after 2-propanol and 2-butanol exposure but to a lesser degree than those observed after ethanol exposure [Fig. 3(c)]. These images also rule out nanoparticle coarsening as deactivation mechanism, since the particle size remains constant after deactivation.

The decrease in activity observed at temperatures higher than 250 °C for 2-propanol and 2-butanol coincides with the onset of water formation. Acidic sites on the ZrO<sub>2</sub> have been reported to enhance the dehydration reactions [66,67,75,77,80,96–99], namely reaction (12) for 2-propanol and reaction (14) for 2-butanol. These reactions would result in the formation of water and the corresponding alkenes, i.e. propene and butene. Therefore, it is possible that as our Pt catalysts become poisoned by carbon deposits, some of the alcohol decomposition activity observed at higher temperatures ( $T > 250$  °C) can be exclusively attributed to the nanocrystalline ZrO<sub>2</sub> support.

The potential use of these reactions may be studied according to the specific application being considered. The dehydrogenation of 2-propanol will occur at the lowest temperature over the Pt/ZrO<sub>2</sub> catalyst as compared to the other reactions, generating H<sub>2</sub> and acetone. This makes 2-propanol a viable candidate for energy applications, particularly in stationary sources as well as industrial settings where both acetone and hydrogen could be recovered and reused. 2-Butanol displays similar properties, generating butanone. However, at approximately 300 °C, methanol decomposition will generate more than twice the amount of hydrogen from the same amount of reactant as any of the other alcohols studied here. Since this reaction generates almost exclusively carbon monoxide for this temperature range, the CO generated could be utilized as a reactant in the water-gas shift reaction, generating even more H<sub>2</sub> and CO<sub>2</sub>. Oxidation and steam reforming reactions involving the alcohols included in this study will most likely continue to grow in importance in the coming years due to their applicability in a wide range of industrial processes, e.g. chemical synthesis and emissions control/material recovery.

## 5. Conclusions

We have conducted a systematic study of the performance of nanoscale Pt/ZrO<sub>2</sub> catalyst for the decomposition of C1–C4 alcohols at temperatures between 100 °C and 400 °C. Our preparation method allowed us to obtain NPs with narrow size distributions, resulting in model material system for our comparative reactivity studies.

The main results derived from the analysis of our data include: (i) the onset temperature for alcohol decomposition (and H<sub>2</sub> generation) increases from propanol  $\leq$  butanol  $<$  methanol  $\leq$  ethanol, ranging from 125 °C to 200 °C; (ii) the maximum alcohol conversion was found to increase from ethanol  $<$  2-butanol  $\leq$  2-propanol  $<$  methanol, ranging from  $\sim$ 47% to 100% in a temperature range of 100–300 °C; (iii) the maximum H<sub>2</sub> production rates followed the same trend as the conversion rates, with a maximum of  $\sim$ 12  $\mu\text{mol}(\text{H}_2)/\text{s g}$  catalyst during methanol decomposition, down to  $\sim$ 3  $\mu\text{mol}(\text{H}_2)/\text{s g}$  catalyst for the ethanol reaction.

High selectivity towards hydrogen production was observed for all the alcohols being decomposed over the Pt/ZrO<sub>2</sub> catalyst. With the exception of methanol, all the studied alcohols caused the catalyst to become deactivated at high temperatures ( $T > 325$  °C for ethanol and  $T > 250$  °C for 2-propanol and 2-butanol) due to the deposition of carbonaceous species over the Pt particles and their ZrO<sub>2</sub> support. The onset of dehydration reactions, possibly over the ZrO<sub>2</sub> support, was observed following indications of catalyst deactivation during 2-propanol and 2-butanol reactions. Optimum temperatures with the highest alcohol-to-H<sub>2</sub> conversions are 300 °C for methanol and ethanol, and 250 °C for 2-propanol and 2-butanol. Under these conditions, the Pt/ZrO<sub>2</sub> catalyst is expected to perform well for an extended period of time.

It should also be noted that the oxidized Pt species originally present in the as prepared samples were found to become significantly reduced in the course of the reactions with the different alcohols. However, additional studies are needed in order to establish correlations between the oxidation state of Pt and its catalytic performance.

## Acknowledgement

We would like to thank Aniruddha Dutta for the analysis of the TEM images and Elaine Zhou for her help with the preparation of these samples. This work was possible thanks to the funding of the Office of Basic Energy Sciences of the US Department of Energy (DE-FG02-08ER15995).

## References

- [1] J.D. Aiken, R.G. Finke, *J. Mol. Catal. A* 145 (1999) 1.
- [2] G.C. Bond (Ed.), *Metal-catalyzed Reactions of Hydrocarbons*, Springer, New York, NY, 2005.
- [3] F.R. Keene, *Coord. Chem. Rev.* 187 (1999) 121.
- [4] B.Z. Zhan, A. Thompson, *Tetrahedron* 60 (2004) 2917.
- [5] H. Hattori, *Appl. Catal. A* 222 (2001) 247.
- [6] J.R. Rostrup-Nielsen, *Phys. Chem. Chem. Phys.* 3 (2001) 283.
- [7] G.A. Deluga, J.R. Salge, L.D. Schmidt, X.E. Verykios, *Science* 303 (2004) 993.
- [8] W.J. Zhou, B. Zhou, W.Z. Li, Z.H. Zhou, S.Q. Song, G.Q. Sun, Q. Xin, S. Douvartzides, A. Goula, P. Tsiakaras, *J. Power Sources* 126 (2004) 16.
- [9] P. Mizsey, E. Newson, T.B. Truong, P. Hottinger, *Appl. Catal. A* 213 (2001) 233.
- [10] A. Kowal, M. Li, M. Shao, K. Sasaki, M.B. Vukmircovic, J. Zhang, N.S. Marinkovic, P. Liu, A.I. Frenkel, R.R. Adzic, *Nat. Mater.* 8 (2009) 325.
- [11] E. Orucu, F. Gokaliler, A.E. Aksoylu, Z.I. Onsan, *Catal. Lett.* 120 (2008) 198.
- [12] K.W. Park, D.S. Han, Y.E. Sung, *J. Power Sources* 163 (2006) 82.
- [13] J. Riberio, D.M. dos Anjos, K.B. Kokoh, C. Coutanceau, J.M. Leger, P. Olivi, A.R. de Andrade, G. Tremilios-Filho, *Electrochim. Acta* 52 (2007) 6997.
- [14] Z.H. Liu, W.Z. Huo, H. Ma, K. Qiao, *Chin. J. Chem. Eng.* 14 (2006) 676.
- [15] H.F. Rase (Ed.), *Handbook of Commercial Catalysts. Heterogeneous Catalysis*, CRC Press, Boca Raton, 2000.
- [16] L. Bromberg, D.R. Cohn, A. Rabinovich, J. Heywood, *Int. J. Hydrogen Energy* 26 (2001) 1115.

- [17] M.A.R.S. Al-Baghdadi, H.A.K.S. Al-Janabi, *Energ. Convers. Manag.* 41 (2000) 77.
- [18] S.R. Segal, K.A. Carrado, C.L. Marshall, K.B. Anderson, *Appl. Catal. A* 248 (2003) 33.
- [19] T. Mizuno, Y. Matsumura, T. Nakajima, S. Mishima, *Int. J. Hydrogen Energy* 28 (2003) 1393.
- [20] N. Palmeri, V. Chiodo, S. Freni, F. Frusteri, J.C.J. Bart, S. Cavallaro, *Int. J. Hydrogen Energy* 33 (2008) 6627.
- [21] N. Meng, S. Shinoda, Y. Saito, *Int. J. Hydrogen Energy* 22 (1997) 361.
- [22] W. Mooksuwan, S. Kumar, *Int. J. Energ. Res.* 24 (2000) 1109.
- [23] M. Borasio, O.R. de la Fuente, G. Rupprechter, H.J. Freund, *J. Phys. Chem. B* 109 (2005) 17791.
- [24] H. Borchert, B. Jurgens, T. Nowitzki, P. Behrend, Y. Borchert, V. Zielasek, S. Giorgio, C.R. Henry, M. Baumer, *J. Catal.* 256 (2008) 24.
- [25] J.C. Brown, E. Gulari, *Catal. Commun.* 5 (2004) 431.
- [26] W.Q. Cao, G.W. Chen, S.L. Li, Q. Yuan, *Chem. Eng. J.* 119 (2006) 93.
- [27] J.R. Croy, S. Mostafa, J. Liu, Y.H. Sohn, B. Roldan Cuenya, *Catal. Lett.* 118 (2007) 1.
- [28] J.R. Croy, S. Mostafa, L. Hickman, H. Heinrich, B. Roldan Cuenya, *Appl. Catal. A* 350 (2008) 207.
- [29] J.R. Croy, S. Mostafa, J. Liu, Y.H. Sohn, H. Heinrich, B. Roldan Cuenya, *Catal. Lett.* 119 (2007) 209.
- [30] M.L. Cubeiro, J.L.G. Fierro, *Appl. Catal. A* 168 (1998) 307.
- [31] M.L. Cubeiro, J.L.G. Fierro, *J. Catal.* 179 (1998) 150.
- [32] S. Imamura, T. Hagashihara, Y. Saito, H. Aritani, H. Kanai, Y. Matsumura, N. Tsuda, *Catal. Today* 50 (1999) 369.
- [33] M.P. Kapoor, Y. Ichihashi, W.J. Shen, Y. Matsumura, *Catal. Lett.* 76 (2001) 139.
- [34] M.P. Kapoor, A. Raj, Y. Matsumura, *Micropor. Mesopor. Mater.* 44 (2001) 565.
- [35] Y.C. Lin, K.L. Hohn, S.M. Stagg-Williams, *Appl. Catal. A* 327 (2007) 164.
- [36] Y. Matsumura, M. Okumura, Y. Usami, K. Kagawa, H. Yamashita, M. Anpo, M. Haruta, *Catal. Lett.* 44 (1997) 189.
- [37] Y. Matsumura, W.J. Shen, *Top. Catal.* 22 (2003) 271.
- [38] S. Shiizaki, I. Nagashima, Y. Matsumura, M. Haruta, *Catal. Lett.* 56 (1998) 227.
- [39] B.E. Traxel, K.L. Hohl, *Appl. Catal. A* 244 (2003) 129.
- [40] R. Ubago-Perez, F. Carrasco-Marin, C. Moreno-Castilla, *Appl. Catal. A* 275 (2004) 119.
- [41] R. Ubago-Perez, F. Carrasco-Marin, C. Moreno-Castilla, *Catal. Today* 123 (2007) 158.
- [42] Y. Usami, K. Kagawa, M. Kawazoe, Y. Matsumura, H. Sakurai, M. Haruta, *Appl. Catal. A* 171 (1998) 123.
- [43] O. Skoplyak, C.A. Menning, M.A. Barteau, J.G. Chen, *J. Chem. Phys.* 127 (2007) 114707.
- [44] J.L. Bi, S.N. Hsu, C.T. Yeh, C.B. Wang, *Catal. Today* 129 (2007) 330.
- [45] A. Yee, S.J. Morrison, H. Idriss, *J. Catal.* 186 (1999) 279.
- [46] M. Domok, M. Toth, J. Rasko, A. Erdohelyi, *Appl. Catal. B* 69 (2007) 262.
- [47] S.M. de Lima, A.M. Silva, U.M. Graham, G. Jacobs, B.H. Davis, L.V. Mattos, F.B. Noronha, *Appl. Catal. A* 352 (2009) 95.
- [48] S.M. de Lima, I.O. da Cruz, G. Jacobs, B.H. Davis, L.V. Mattos, F.B. Noronha, *J. Catal.* 257 (2008) 356.
- [49] V.V. Galvita, V.D. Belyaev, V.A. Semikolenov, P. Tsiakaras, A. Frumin, V.A. Sobyannin, *React. Kinet. Catal. Lett.* 76 (2002) 343.
- [50] S.N. Hsu, J.L. Bi, W.F. Wang, C.T. Yeh, C.B. Wang, *Int. J. Hydrogen Energy* 33 (2008) 693.
- [51] G. Jacobs, R.A. Keogh, B.H. Davis, *J. Catal.* 245 (2007) 326.
- [52] A.F. Lee, D.E. Gawthrope, N.J. Hart, K. Wilson, *Surf. Sci.* 548 (2004) 200.
- [53] J. Llorca, P.R. de la Piscina, J. Sales, N. Homs, *Chem. Commun.* (2001) 641.
- [54] L.V. Mattos, E. Noronha, *J. Catal.* 233 (2005) 453.
- [55] L.V. Mattos, F.B. Noronha, *J. Power Sources* 145 (2005) 10.
- [56] R.M. Navarro, M.C. Alvarez-Galvan, M.C. Sanchez-Sanchez, F. Rosa, J.L.G. Fierro, *Appl. Catal. B* 55 (2005) 229.
- [57] T. Nishiguchi, T. Matsumoto, H. Kanai, K. Utani, Y. Matsumura, W.J. Shen, S. Imamura, *Appl. Catal. A* 279 (2005) 273.
- [58] P.Y. Sheng, W.W. Chiu, A. Yee, S.J. Morrison, H. Idriss, *Catal. Today* 129 (2007) 313.
- [59] E. Vesselli, G. Coslovich, G. Comelli, R. Rosei, *J. Phys.: Cond. Matter* 17 (2005) 6139.
- [60] R. Ianniello, V.M. Schmidt, J.L. Rodriguez, E. Pastor, *J. Electroanal. Chem.* 471 (1999) 167.
- [61] O. Skoplyak, M.A. Barteau, J.G. Chen, *J. Phys. Chem. B* 110 (2006) 1686.
- [62] Y.Z. Yang, C.H. Chang, H. Idriss, *Appl. Catal. B* 67 (2006) 217.
- [63] S. Duan, S. Senkan, *Ind. Eng. Chem. Res.* 44 (2005) 6381.
- [64] S.M. de Lima, A.M. Silva, I.O. da Cruz, G. Jacobs, B.H. Davis, L.V. Mattos, F.B. Noronha, *Catal. Today* 138 (2008) 162.
- [65] J.N. Keuler, L. Lorenzen, *J. Membr. Sci.* 202 (2002) 17.
- [66] E.M. Gaigneaux, P.E. Tsiakaras, D. Herla, L. Ghenne, P. Ruiz, B. Delmon, *Catal. Today* 33 (1997) 151.
- [67] J.N. Keuler, L. Lorenzen, S. Miachon, *Appl. Catal. A* 218 (2001) 171.
- [68] P.J. Skrdla, R.T. Robertson, *J. Mol. Catal. A* 194 (2003) 255.
- [69] P.J. Skrdla, C. Lindemann, *Appl. Catal. A* 246 (2003) 227.
- [70] K. Elkabouss, M. Kacimi, M. Ziyad, S. Ammar, F. Bozon-Verduraz, *J. Catal.* 226 (2004) 16.
- [71] R. Valarivan, C.N. Pillai, C.S. Swamy, *React. Kinet. Catal. Lett.* 53 (1994) 429.
- [72] J.Z. Gao, F. Guan, Y.C. Zhao, W. Yang, Y.J. Ma, X.Q. Lu, J.G. Hou, J.W. Kang, *Mater. Chem. Phys.* 71 (2001) 215.
- [73] J.E. Herrera, J.H. Kwak, J.Z. Hu, Y. Wang, C.H.F. Peden, J. Macht, E. Iglesia, *J. Catal.* 239 (2006) 200.
- [74] Z.L. Wang, Q.S. Liu, H.F. Yu, T.H. Wu, G.J. Wang, *Appl. Catal. A* 239 (2003) 87.
- [75] C.D. Baertsch, K.T. Komala, Y.H. Chua, E. Iglesia, *J. Catal.* 205 (2002) 44.
- [76] Z.L. Wang, H.C. Ma, W.C. Zhu, G.J. Wang, *React. Kinet. Catal. Lett.* 76 (2002) 271.
- [77] J. Macht, C.D. Baertsch, M. May-Lozano, S.L. Soled, Y. Wang, E. Iglesia, *J. Catal.* 227 (2004) 479.
- [78] S. Lambert, C. Cellier, F. Ferauche, E.M. Gaigneaux, B. Heinrichs, *Catal. Commun.* 8 (2007) 2032.
- [79] R.M. Rioux, M.A. Vannice, *J. Catal.* 234 (2005) 247.
- [80] R.M. Rioux, M.A. Vannice, *J. Catal.* 233 (2005) 147.
- [81] L.K. Ono, D. Sudfeld, B. Roldan Cuenya, *Surf. Sci.* 600 (2006) 5041.
- [82] B.V. Crist (Ed.), *On-Screen PDF Handbook of Monochromatic XPS Spectra—Commercially Pure Binary Oxides*, Vol. 2, XPS International Inc., 2005, p. 828.
- [83] NIST X-ray Photoelectron Spectroscopy Database. Version 3.4 (Web Version). <http://srdata.nist.gov/xps/index.htm>.
- [84] A.K. Shukla, A.S. Arico, K.M. El-Khatib, H. Kim, P.L. Antonucci, V. Antonucci, *Appl. Surf. Sci.* 137 (1999) 20.
- [85] F. Sen, G. Gokagac, *J. Phys. Chem. C* 111 (2007) 5715.
- [86] W. Eberhardt, P. Fayet, D.M. Cox, Z. Fu, A. Kaldor, R. Sherwood, D. Sondericker, *Phys. Rev. Lett.* 64 (1990) 780.
- [87] S.T. Srinivas, P.K. Rao, *J. Catal.* 179 (1998) 1.
- [88] J.R. Croy, S. Mostafa, H. Heinrich, B. Roldan Cuenya, *Catal. Lett.* 131 (2009) 21.
- [89] Z. Paal, U. Wild, M. Muhler, J.M. Manoli, C. Potvin, T. Buchholz, S. Sprenger, G. Resofszki, *Appl. Catal. A* 188 (1999) 257.
- [90] F.B. Noronha, E.C. Fendley, R.R. Soares, W.E. Alvarez, D.E. Resasco, *Chem. Eng. J.* 82 (2001) 21.
- [91] M.D. Appay, J.M. Manoli, C. Potvin, M. Muhler, U. Wild, O. Pozdnyakova, Z. Paal, *J. Catal.* 222 (2004) 419.
- [92] A. Erdohelyi, J. Rasko, T. Kecskes, M. Toth, M. Domok, K. Baan, *Catal. Today* 116 (2006) 367.
- [93] D. Haffad, A. Chambellan, J.C. Lavalley, *J. Mol. Catal. A* 168 (2001) 153.
- [94] D. Kulkarni, S.E. Wachs, *Appl. Catal. A* 237 (2002) 121.
- [95] R.M. Mohamed, *J. Mater. Process Technol.* 209 (2009) 577.
- [96] M.K. Weldon, C.M. Friend, *Chem. Rev.* 96 (1996) 1391.
- [97] Q. Zhuang, J.M. Miller, *Appl. Catal. A* 209 (2001) L1.
- [98] M.E. Manriquez, T. Lopez, R. Gomez, J. Navarrete, *J. Mol. Catal. A* 220 (2004) 229.
- [99] G. Larsen, E. Lotero, L.M. Petkovic, D.S. Shobe, *J. Catal.* 169 (1997) 67.